Neuron, Vol. 21, 581–591, September, 1998, Copyright ©1998 by Cell Press

Novel Anchorage of GluR2/3 to the Postsynaptic Density by the AMPA Receptor–Binding Protein ABP

S. Srivastava,* P. Osten,* F. S. Vilim,*§ L. Khatri,* G. Inman,*‖ B. States,* C. Daly,* S. DeSouza,* R. Abagyan,† J. G. Valtschanoff,‡ R. J. Weinberg,‡ and E. B. Ziff*#

*Howard Hughes Medical Institute
and Department of Biochemistry
New York University Medical Center
New York, New York 10016
†and Skirball Institute
Department of Biochemistry
New York University Medical Center
New York, New York 10016
and Courant Institute of Mathematics
New York University
New York, New York 10012
‡Department of Cell Biology and Anatomy
University of North Carolina
Chapel Hill, North Carolina 27599

Summary

We report the cloning of α-amino-3-hydroxy-5-methyl-4-isoxazole propionic acid (AMPA) receptor–binding protein (ABP), a postsynaptic density (PSD) protein related to glutamate receptor–interacting protein (GRIP) with two sets of three PDZ domains, which binds the GluR2/3 AMPA receptor subunits. ABP exhibits widespread CNS expression and is found at the postsynaptic membrane. We show that the protein interactions of the ABP/GRIP family differ from the PSD-95 family, which binds N-methyl-D-aspartate (NMDA) receptors. ABP binds to the GluR2/3 C–terminal VKI-COOH motif via class II hydrophobic PDZ interactions, distinct from the class I PSD-95–NMDA receptor interaction. ABP and GRIP also form homo- and heteromultimers through PDZ–PDZ interactions but do not bind PSD-95. We suggest that the ABP/GRIP and PSD-95 families form distinct scaffolds that anchor, respectively, AMPA and NMDA receptors.

Introduction

At excitatory synapses, the binding of glutamate to ionotropic and metabotropic glutamate receptors triggers the ionic fluxes and biochemical cascades that are the basis of chemical synaptic signaling. Two major classes of ionotropic glutamate receptors characterized by their selective affinity for N-methyl-D-aspartate (NMDA) and α-amino-3-hydroxy-5-methyl-4-isoxazole propionic acid (AMPA) colocalize at excitatory synapses but display significant functional and structural differences. AMPA receptors, which are formed from GluR1–GluR4 (GluR A–D) subunits (Hollmann and Heinemann, 1994), mediate fast excitatory transmission, while NMDA receptors, which are assembled from the NR1 and NR2A-D subunits, may provide synaptic modification through their ability to admit Ca^{2+} ions (McBain and Mayer, 1994). In one model for synaptic plasticity, functionally "silent" synapses bearing NMDA receptors are activated through the synaptic insertion or activation of AMPA receptors by an NMDA receptor–dependent mechanism (Maren et al., 1993; Isaac et al., 1995; Liao et al., 1995; Malenka and Nicoll, 1997). This model implies that the AMPA and NMDA receptors undergo different forms of processing prior to functioning at synapses. Indeed, AMPA receptors are transported to synapses prior to NMDA receptors (Rao et al., 1998), are less firmly anchored to subsynaptic structures (Allison et al., 1998), and have a different distribution within the postsynaptic membrane, relative to NMDA receptors (Kharazia and Weinberg, 1997; Somogyi et al., 1998). It is now evident that essential aspects of AMPA and NMDA receptor localization and regulation are determined by the interaction of the intracellular receptor C terminus of the receptor with anchoring and regulatory proteins present in the postsynaptic density (PSD) (Kennedy, 1997; Ziff, 1997).

NMDA receptors are anchored at synapses by the PSD-95 family, a subset of the "membrane-associated guanylate kinases" (MAGUKs), so named because they contain a guanylate kinase–related domain (Anderson, 1996). PSD-95 (SAP90) and related proteins bind to NR2 and NR1 C termini through 80–90 amino acid motifs called PDZ domains, three of which are present in the PSD-95 N-terminal region (Cho et al., 1992; Kistner et al., 1993; reviewed by Ehlers et al., 1996; Gomperts, 1996). PDZ domains have a globular structure (Cabral et al., 1996; Doyle et al., 1996) and are known to mediate protein–protein interactions with the extreme C termini of the target proteins. The PDZ domains of the PSD-95 family bind to the S/T-X-V motif at the C terminus of the NMDA receptor (Kornau et al., 1995; Kim et al., 1996; Lau et al., 1996; Niethammer et al., 1996) and can induce NMDA receptor clustering (Kim et al., 1996; Sheng and Wyszynski, 1997).

Recently, a new PDZ protein, glutamate receptor–interacting protein (GRIP), which binds to GluR2 and GluR3 subunits, has been proposed to serve an analogous anchoring function for AMPA receptors (Dong et al., 1997). Here, we report the cloning of a novel PSD protein, ABP (AMPA receptor–binding protein), which also binds to the C termini of the GluR2 and GluR3 AMPA receptor subunits via PDZ domains. We show that the ABP/GRIP and PSD-95 families establish selective protein interactions by binding, respectively, with AMPA and NMDA receptors and by formation of family-specific multimers. These two families thus establish distinct scaffolds that anchor AMPA and NMDA receptors at the synapse. We suggest that the molecular features of receptor–PSD protein interactions may contribute to the differential processing of AMPA and NMDA receptors.

§Present address: Department of Physiology and Biophysics, Mount Sinai School of Medicine, New York, New York 10029.
‖Present address: Ludwig Institute for Cancer Research, St. Mary's Hospital Medical School, London W21PG, United Kingdom.
#To whom correspondence should be addressed.

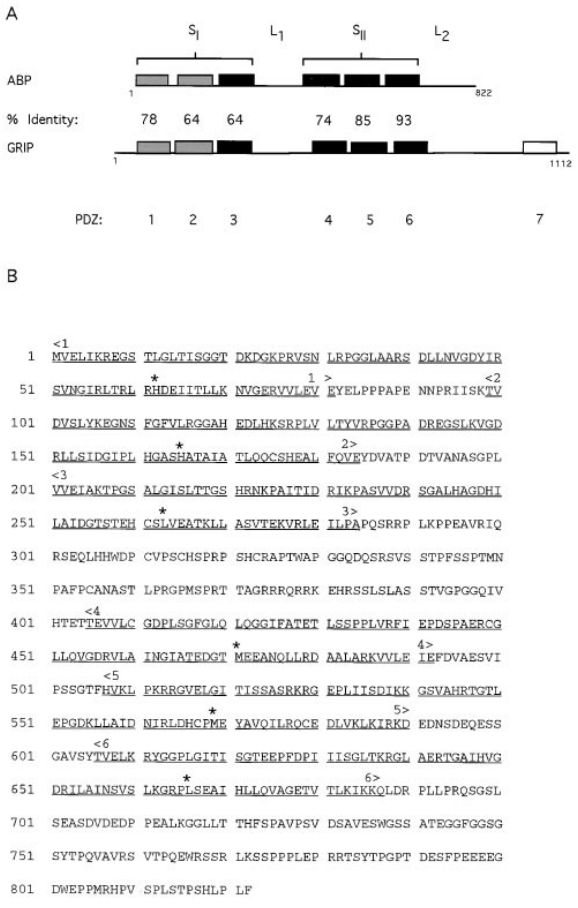

Figure 1. Structure of ABP Protein and Relationship to GRIP

(A) Comparison of the structures of the ABP and GRIP proteins, including the extent of sequence identities between corresponding PDZ domains. PDZ domains with a His at the αB1 residue position are shown as gray boxes and those with a hydrophobic residue (Met or Leu) as solid boxes. PDZ7 of GRIP has a Cys residue at αB1. The positions of PDZ domain sets S_I and S_{II} and linkers L_1 (122 amino acids) and L_2 (135 amino acids) are indicated.

(B) Amino acid sequence of ABP with the positions of PDZ domains 1–6 underlined and PDZ domain right (<) and left (>) boundaries marked. The αB1 residues are indicated by asterisks.

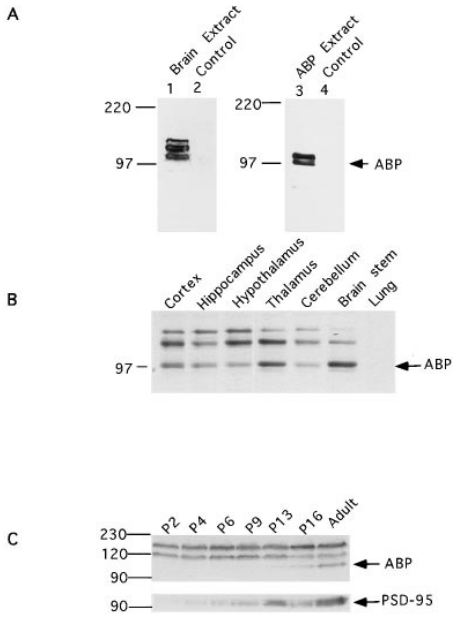

Figure 2. Brain-Specific Expression of ABP in Rat Tissues and Developmental Regulation

(A) Whole adult rat brain extract was Western blotted with affinity-purified α ABP L_2 antiserum. Peptide species of 130, 120, and 98 kDa were detected and were specifically competed by preabsorbtion of the serum with antigen peptide (lane 2). The 98 kDa peptide comigrated with the upper band of a doublet encoded by the ABP cDNA in transfected 293T cells (lane 3). which were both competed by peptide preabsorbtion (lane 4).

(B) Tissue distribution of ABP protein. A Western blot of 100 μg of homogenates of indicated rat brain tissues was probed with affinity-purified ABP L_2 antiserum. ABP is detected in all brain tissues but not in lung.

(C) Developmental expression of ABP protein. A Western blot of homogenates of developing rat brain (50 μg) from rats of the indicated ages was probed with affinity-purified ABP L_2 antiserum. ABP protein levels increase rapidly starting at P9, with maximal expression in adult. The same blot, stripped and reprobed with a monoclonal antibody against PSD-95 or GluR2 (data not shown), revealed PSD-95 expression from P4 and GluR2 from P2.

Results

To identify proteins that interact with the GluR2 C terminus, we used the last 50 amino acids of GluR2 as bait to screen an adult rat brain library using the yeast two-hybrid technique (Fields and Song, 1989). Three clones that encoded proteins with PDZ domains were isolated. Two identical clones encoded a five–PDZ domain fragment (PDZ2–PDZ6) of a novel protein, ABP. The third clone encoded a five PDZ domain fragment (PDZ3–PDZ7) of the recently identified GluR2/3 binding protein GRIP (Dong et al., 1997). By screening an adult rat brain library, we isolated the full-length ABP clone of 5,422 base pairs with an open reading frame (ORF) of 822 amino acids. Because there are similarities between the GRIP ORF and the untranslated 5′ region of ABP, we confirmed the ORF of ABP by screening other libraries. Sequencing revealed that ABP and GRIP have related structural organizations (Figure 1). The first six PDZ domains of both proteins are arranged in two clusters, with three PDZ domains in each cluster (PDZ domain sets I and II, S_I and S_{II}). These clusters are followed by two linker regions, linker 1 (L_1) and linker 2 (L_2), respectively.

ABP Is Brain Specific and Regulated in Development

ABP mRNA is widely expressed in the nervous system, including cortex, hippocampus, striatum, thalamus, hypothalamus, cerebellum, and brainstem. Low levels were found in heart, but *ABP* mRNA could not be detected in testis, lung, or in other nonneuronal tissues (data not shown). Western blotting with an affinity-purified antiserum directed to an ABP L_2 peptide (Figure 2A) whose sequence is not present in GRIP and does not show any cross-reactivity with transfected GRIP protein (data not shown) detected three bands in adult brain extract migrating at 130, 120, and 98 kDa (lane 1), all of which were competed by antigen peptide (lane 2) but

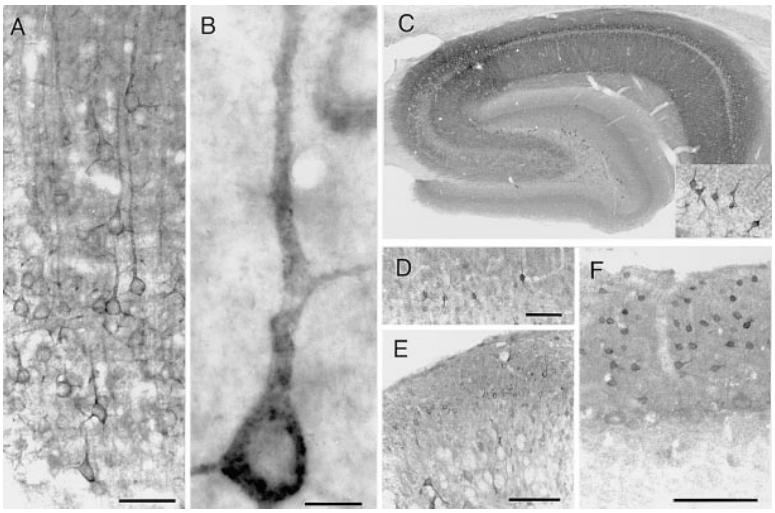

Figure 3. Localization of ABP in CNS Neurons

The distribution of ABP was determined in parasagittal and coronal sections from brain and transverse sections from spinal cord at lumbar level. Sections of rat brain (40 μm) or spinal cord were labeled with affinity-purified ABP L_2 sera and viewed in bright field by DAB as described in Experimental Procedures.

(A) Adult rat cortex; staining of layer III pyramids.

(B) High magnification view of a cortical pyramidal cell.

(C) Hippocampal overview; maximal staining in interneurons of dentate gyrus (see inset) and CA1–CA2 border.

(D) Nonpyramidal neurons in upper layers of cortex.

(E) Staining in superficial layers of spinal dorsal horn.

(F) Stellate cells in the molecular layer of cerebellum.

Scale bars, 50 μm (A), 20 μm (B), and 100 μm (C–F).

not by an unrelated peptide (data not shown). The smallest, the 98 kDa band, comigrated with one band of a doublet encoded by the ABP cDNA in transfected 293T cells (lanes 3 and 4), identifying the 98 kDa peptide as the 822 amino acid ABP. The three bands were detected in cortex, hippocampus, thalamus, cerebellum, and brain stem but not lung (Figure 2B) or liver (data not shown). Since the three bands copurify in brain subcellular fractions (see below), show brain-specific coexpression, and are detected by different ABP-specific antisera (see Discussion), we conclude that they are closely related peptides. Reprobing the blot with a GluR2-specific serum confirmed that all of the ABP-positive tissues expressed GluR2 (data not shown). During development, the 98 kDa band is expressed at low levels prior to postnatal day 9 (P9), whereupon its expression increases, with the highest levels detected in the adult (Figure 2C). GluR2 was detected in this experiment as early as P2 (data not shown), and PSD-95 was detected at P4 (Figure 2C; Cho et al., 1992). Thus, GluR2 and PSD-95 expression precede expression of the 98 kDa ABP band. In contrast, the 120 and 130 kDa ABP-related bands are expressed at roughly constant levels from P2 to adult.

ABP is detected by immunocytochemistry throughout the brain, but it is concentrated in specific loci (Figure 3). ABP is seen cytoplasmically in perikarya and proximal dendrites of many neurons, and staining is generally excluded from nuclei. This staining was blocked by omission of primary antiserum or by preincubation of the antiserum with its peptide conjugate at dilutions as low as 1:50,000 (data not shown). In neocortex, staining is prominent in layer III pyramidal neurons (Figures 3A and 3B) and in large nonpyramidal neurons in layer III (Figure 3D) and also a in few neurons in layer I. Sparse nonpyramidal neurons in deeper layers of cortex are strongly stained. The hippocampal formation shows considerable staining (Figure 3C), especially in the pyramidal neurons of CA2. Some interneurons also stain intensely, especially in the stratum radiatum of Ammon's horn and in the granular layer of the dentate gyrus. Numerous small neurons in superficial layers of the dorsal horn are strongly positive (Figure 3E). In cerebellum, stellate cells in the molecular layer stain strongly, in contrast to weak staining in Purkinje and granule cells (Figure 3F). Several other cell types in the brain show positive immunoreactivity for ABP, including large multipolar (probably cholinergic) neurons in basal forebrain and striatum, cells in the islets of Calleja, numerous cells of the pars compacta of the substantia nigra, the large cells in pars reticulata, motor nuclei of brain stem (V and VII), and motoneurons in the spinal cord. In addition to this cellular staining, considerable staining is seen in neuropil, either diffuse or in small punctae, suggesting possible synaptic localization.

Synaptic Localization of ABP

To confirm the synaptic localization of ABP, we made subcellular fractions of adult rat forebrain. ABP and the related 120 and 130 kDa bands were present in whole forebrain extract and were enriched in synaptosomes and synaptosomal membranes but were depleted in the synaptosomal soluble fraction. ABP was most highly enriched in the PSD fraction, where it copurified with the 120 and 130 kDa peptide bands and with GluR2, which is also enriched in the PSD fraction (Hampson et al., 1992; Hayashi et al., 1997) (Figure 4A). The specificity of the fractionation was confirmed by the findings that αCaM kinase, which is present in both soluble and PSD-associated forms, was detected in both the soluble synaptosome and in PSD fractions, while synapsin, which is presynaptic, was enriched in synaptosomes and synaptosomal membrane but was absent from the PSD (data not shown).

To establish the synaptic colocalization of ABP, the distribution of ABP was examined by electron microscopy of immunogold-labeled sections of adult rat brain. This confirmed that ABP is present at the postsynaptic membrane of excitatory synapses (Figure 4B). In blocks from layers II–III of somatic sensory cortex and from stratum radiatum of hippocampal CA2, gold particles

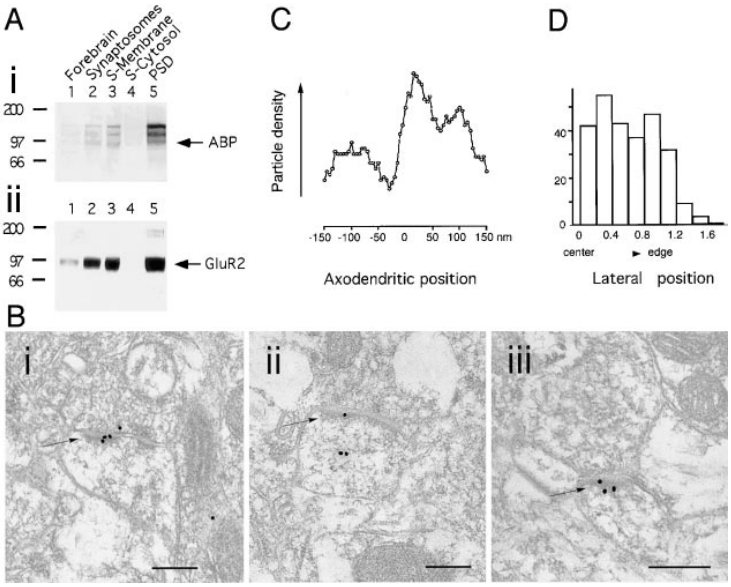

Figure 4. ABP Is Located at Synaptic Junctions

(A) Immunoblots of subcellular fractions were prepared (50 μg) as described in Experimental Procedures.
Lanes:
(1) Adult forebrain extract.
(2) Synaptosomes.
(3) Synaptosomal membrane.
(4) Synaptosomal cytosol.
(5) PSD fraction.
(i) ABP protein detected with affinity-purified ABP L_2 sera.
(ii) The same blot was stripped and reprobed with GluR2 antibody. ABP is enriched in synaptosomes and in the PSD fraction together with the 120 and 130 kDa peptides and copurifies with GluR2.
(B) Electron micrographs of thin sections of layers II–III of somatic sensory cortex and stratum radiatum of hippocampal CA2 immunolabeled with 18 nm gold particles; labeling is primarily associated with asymmetric synapses. PSD is indicated by arrows. Scale bars, 200 nm.
(i) Perforated axospinous synapse in neocortex is strongly immunopositive for ABP.
(ii) Neocortex labeling at PSD and also associated with cytoskeletal elements inside dendritic spine.
(iii) Immunopositive axospinous synapse in stratum radiatum of CA2 region of hippocampus.
(C) Distribution of immunogold labeling along the axodendritic axis (zero corresponds to the outer leaflet of the postsynaptic membrane). Graph was constructed by pooling distance measurements (from the center of each gold particle to the membrane) from 272 particles into 5 nm bins; data were smoothed with a five-point running average. Zero on the ordinate corresponds to the vertical line of the x-axis. Labeling is mainly dendritic, concentrated 10–30 nm inside the membrane, roughly corresponding to the region of the PSD.
(D) Distribution of labeling along axis parallel to the membrane. Lateral position of the projection of the particle along synaptic membrane was normalized; zero corresponds to the center of the active zone, 1.0 to its edge (see text for details). Histogram shows binned data from the same particles as in (A).

coding for ABP showed a clear association with asymmetric synapses, though not all synapses were labeled. Synaptic labeling for ABP was concentrated over the postsynaptic membrane and the PSD, extending (at lower concentration) into the cytoplasm adjacent to the PSD, and it was generally sparser over the synaptic cleft and the presynaptic profile. Labeling could also be seen (at a considerably lower level) adjacent to nonsynaptic plasma membranes and over the outer membrane of mitochondria. Some labeling unrelated to synapses was found in dendrites, where gold particles were associated with microtubules and fragments of endoplasmic reticulum (ER), and dendritic spines, where labeling could be seen over the spine apparatus. To provide quantitative assessment of the staining pattern, we counted gold particles associated with synapses in 60 randomly selected fields from three animals. Labeling was at its highest concentration 15–30 nm inside the postsynaptic membrane, extending ~100 nm into the cytoplasm (Figure 4C). Examining labeling on the "lateral" axis (tangential to the synaptic membrane), particles within 40 nm of the postsynaptic membrane were almost completely confined to the synaptic active zone (Figure 4D). This association was less pronounced for particles further away from the membrane. In perikarya, low levels of labeling were seen over nuclei, mitochondria, and ER. When primary antibody was omitted, gold particles were completely absent or very rare. When normal serum was substituted for primary, sparse gold particles appeared scattered at random, showing no significant affinity for synapses.

Specificity of ABP–GluR2 Interaction

We next determined the ability of ABP to bind AMPA and NMDA receptor subunits. Using yeast interaction assays, we established that ABP binds selectively to the GluR2 and GluR3 C termini but not to GluR1, GluR4, or NR2A C termini (Table 1). We confirmed the specificity of ABP–GluR2 interaction in another system by coexpressing these proteins in 293T cells. Both ABP and the ABP L_1–S_{II}–L_2 fragment bound to GluR2 (Figure 5A, lanes 3 and 4) but not to GluR1 (lanes 1 and 2). Protein expression was confirmed for each transfection (lanes 5–12). We then identified the binding sites on GluR2 (Table 1) and on ABP (Table 2). We found that the last 13 amino acids of the GluR2 C terminus, which are identical in the GluR3 C terminus, were sufficient to bind ABP (Table 1). PDZ domains 3, 5, and 6 of ABP were capable of binding GluR2 but not NR2A (Table 2). These data demonstrate that ABP binds specifically to the C terminus of GluR2/3.

Hydrophobic PDZ–GluR2 Interaction

The PDZ domain is a compactly folded 80–90 amino acid structure with a hydrophobic pocket that binds the peptide C terminus (Cabral et al., 1996; Doyle et al., 1996). Two classes of PDZ domains have been defined based on their binding specificity, determined by residue 1 of α helix–B (residue αB1) in the hydrophobic pocket that interacts directly with the bound peptide (Songyang et al., 1997). Class I PDZ domains that are found in the MAGUKs have a histidine (His) at the αB1

Table 1. Yeast Interaction Assays of Binding of ABP to Glutamate Receptor Subunit Wild-Type and Truncation Mutant C-terminal Sequences

Receptor C terminus Bait Sequence*	ABP receptor C terminus⁺ Interaction Phenotype
GluR1(809)E–(889)L (-SHSSGMPLGATGL-COOH)**	−
GluR2(813)E–(862)I (-EGYNVYGIESVKI-COOH)**	+
GluR3(817)E–(866)I (-EGYNVYGTESVKI-COOH)**	+
GluR4(814)E–(881)P (-QSSGLAVIASDLP-COOH)**	−
NR2A(1369)H–1465(V) (-VYKKMPSIESDV-COOH)**	−
GluR2(813)E–(826)K	−
(813)E–(833)N	−
(813)E–(845)F	−
(827)V–(845)F	−
(834)I–(848)Y	−
(827)V–(862)I	+
(840)Q–(862)I	+
(849)K–(862)I	+/−

Binding was measured by the yeast mating assay using the Matchmaker Two kit (Clonetech) according to the manufacturer's protocol. The receptor C terminal domains were the bait and the ABP protein, lacking a portion of PDZ1, was the interactor. Matings were performed on 10 mM aminotriazole (AT) plates. The +/− phenotype of GluR2(849)K–(862)I is attributed to the short length of its bait sequence. All other phenotypes were distinct.

* The control baits PAS2 empty vector, Myc, p53 and pLAM did not interact.

⁺ Amino acid numbering for GluR subunits refers to the flop form.

** Subunit C-terminal 13 amino acid sequence.

position. This His hydrogen bonds to Ser or Thr at the −2 position of the peptide terminus (Doyle et al., 1996). In the class II PDZ domains, the αB1 residue is hydrophobic.

Sequence alignment (Figure 1B) revealed that PDZ1 and PDZ2 of ABP are class I domains (αB1 is His), while PDZ3, PDZ4, PDZ5, and PDZ6 are class II (αB1 are, respectively, Leu, Met, Met, and Leu). Thus, all of the PDZ domains of ABP that bind to GluR2 are class II domains (see Table 2). PDZ4, although a class II domain, did not bind to GluR2, perhaps because of an anomalous carboxylate loop (S. S. and E. Z., unpublished data).

To analyze the binding specificity further, we mutated GluR2-terminal residues one at a time to alanine (Ala) and coexpressed the point mutants with ABP in 293T cells. Complexes containing epitope-tagged ABP were isolated by immune precipitation and assayed for GluR2 by Western blotting (Figure 5B). Wild-type GluR2 and the mutant K861A, in which Lys at position −1 was changed to Ala, bound to ABP (lanes 1 and 3). Mutants V860A and I862A, in which the 0 and −2 residues, respectively, were changed to Ala, did not form GluR2 complexes (lanes 2 and 4). These results were also confirmed when GluR2 antibody was used to isolate complexes (Figure 5C). We conclude that the 0 and −2 amino acid positions of GluR2 are critical for binding ABP, as seen before for the NMDA receptor and PSD-95 interaction (Kornau et al., 1995).

Since the removal of the two hydrophobic CH_3 moieties of the Val side chain in mutant V860A disrupted ABP binding, these methyl groups appear to be essential to the GluR2–ABP interaction. We examined the role of the methyl groups in binding by modeling the ABP PDZ5–GluR2 complex through homology with the three-dimensional crystallographic structure of a complex of peptide with PDZ3 domain from PSD-95 (Doyle et al., 1996) (Figure 6A) using the ICM-HOMOLOGY method (Cardozo et al., 1995). Although the two PDZ domains have a low sequence identity (28%), the alignment contained only one three-residue deletion (GST) in the loop between the first and the second β strands. The side chains were optimally placed (Cardozo et al., 1995), and the six residues flanking the deleted loop were globally refined. The model was refined together with the GluR2 C–terminal ESVKI pentapeptide. The peptide backbone was tethered to occupy the same position as the backbone of the AQTSV peptide cocrystallized with PDZ3 of PSD-95, while the side chains of the peptide were globally optimized together with the surrounding PDZ side chains (Figure 6B). In the optimal conformation, residues Met 569 and Val −2 form a hydrophobic contact involving the Val methyl groups (Figure 6C) as predicted for a class II interaction. This model could explain the disruption of the complex between GluR2 and ABP by mutagenesis of the Val side chain.

ABP Homomultimerizes and Heteromultimerizes with GRIP via PDZ Domain S_{II}

PSD-95 and its family members multimerize through interactions between N-terminal cysteines (Hsueh et al., 1997) and interact with GKAP through the GK domain (Kim et al., 1997; Naisbitt et al., 1997), which is located at the C terminus. We asked whether ABP and GRIP could also multimerize within their own family. We used the yeast interaction assay to check for a direct interaction between ABP and GRIP (Table 3). We found that S_{II} was sufficient for homo- or heteromultimerization. To confirm the interaction in another system, we coexpressed epitope-tagged ABP (ABP-FLAG) or tagged ABP subdomains (Figure 7) together with epitope-tagged GRIP (GRIP-myc) and assayed for complexes by coimmune precipitation and Western blotting. In the first experiment, GRIP-myc formed a complex with ABP-FLAG but not with PSD-95 (Figure 7A, lanes 1 and 2). We next expressed tagged fragments of ABP with either ABP-FLAG or GRIP-myc. ABP fragment S_{II} multimerized with ABP (Figure 7B, lanes 1 and 2) and GRIP (data not shown) as well as with S_{II}–L_2 and L_I–S_{II}–L_2 (Figure 7C, lanes 1 and 2). This demonstrates that S_{II} is sufficient to bind to ABP itself and to GRIP. As a second test of whether ABP and GRIP can associate in heterologous cells, we expressed ABP and GRIP in COS7 cells. When expressed by themselves, they show a distribution of tiny microaggregates, and in a few cells, a large accumulation can be seen in some intracellular organelles (Figures 7D*i* and 7D*ii*). When ABP and GRIP were coexpressed, there was a dramatic redistribution of both of the proteins in large plaque-like aggregates (Figures 7D*iii* and 7D*iv*). This redistribution suggests that ABP and GRIP can homo- or heteromultimerize to form large scaffolds.

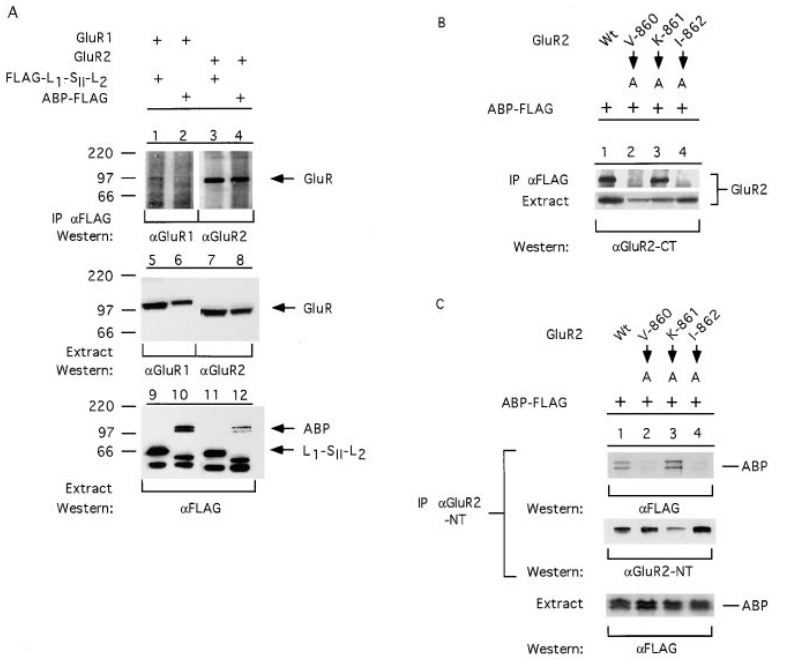

Figure 5. Specificity of Interaction of ABP with the GluR2 C Terminus

(A) Coimmune precipitation of ABP and the L_1–S_{II}–L_2 ABP fragment with AMPA receptor subunits expressed in 293T cells. The GluR1 and GluR2 AMPA receptor subunits were expressed in 293T cells together with FLAG epitope–tagged ABP or L_1–S_{II}–L_2 fragment. Cell extracts were prepared and immune precipitated with anti-FLAG antibody. The presence of associated receptor subunits was assayed by Western blotting. Although no GluR1 complexes with ABP or L_1–S_{II}–L_2 were detected (lanes 1 and 2), GluR2 complexes were observed in both cases (lanes 3 and 4). Western blotting confirmed the expression of GluR1 (lanes 5 and 6), GluR2 (lanes 7 and 8), ABP (lanes 9 and 10), and L_1–S_{II}–L_2 (lanes 11 and 12) in the transfected cells.

(B) Mutation of individual C-terminal residues of GluR2 selectively disrupt binding of ABP. Wild-type (wt) GluR2 or GluR2 mutated to Ala at residues 860, 861, and 862 (lanes 1–4) was coexpressed with ABP-FLAG in 293T cells. Cell extracts were prepared, and ABP complexes were immune precipitated with α FLAG and assayed for the presence of GluR2 by Western blotting with αGluR2 C terminus antibody.

(C) GluR2 was precipitated with αGluR2 N terminus antibody and the presence of ABP assayed by Western analysis with α FLAG antibody. Western blotting of whole-cell extracts confirmed that expression in each transfection was similar. V860 and I862 of GluR2 are essential for binding ABP.

Discussion

We have cloned a new component of the PSD, ABP, which is related to GRIP (Dong et al., 1997). ABP and GRIP form a specialized AMPA receptor–interacting family that selectively binds to GluR2/3 subunits. GluR2, in its most prevalent edited form, makes AMPA channels impermeable to Ca^{2+} (Jonas et al., 1994; Seeburg, 1996). Therefore, through their ability to bind to GluR2, ABP and GRIP may function in the localization and regulation of Ca^{2+}-impermeable AMPA channels.

Three ABP-related peptides are detected by independent ABP sera in brain extract Western blots (Figure 2A and S. S. and E. Z., unpublished data). Since the three peptides copurify in the PSD fraction of rat forebrain and are coexpressed in all brain tissues examined but are absent from liver and lung, the three are probably closely related isoforms encoded by the same gene. This relationship is supported by the recent cloning of the mRNA for an ABP splice isoform that migrates at 130 kDa and encodes a seventh PDZ domain (S. DeS. and E. Z., unpublished data). Thus, ABP is expressed in at least two forms, the six PDZ form analyzed here and a form with seven PDZ domains that is directly analogous to GRIP in structure. ABP and GRIP are closely related with 64%–93% amino acid homology in the six PDZ domains. The high conservation of PDZ domain sequences, including identical αB1 residues for all but PDZ4, suggests that the two proteins have similar PDZ interaction specificities. To understand why both ABP and GRIP are present in the PSD will require elucidation of the functional differences between the two proteins. These differences may include binding of distinct signaling or cytoskeletal proteins, thereby resulting in differential regulation of AMPA receptor function.

Table 2. Binding of Individual PDZ Domains of ABP and PSD-95 to Glutamate Receptor Subunit C-Terminal Sequences

	PDZ Receptor C Terminus* Interaction Phenotype		
PDZ Domain	GluR2	NR2A	PDZ Domain αB1 Amino Acid**
ABP:			
PDZ1(1)M–(81)E	nd	nd	Histidine
PDZ2(99)T–(190)P	−	−	Histidine
PDZ3(196)A–(287)S	++	−	Leucine
PDZ4(405)T–(495)V	−	−	Methionine
PDZ5(507)H–(590)D	++++	−	Methionine
PDZ6(604)S–(687)Q	++	−	Leucine
PSD95:			
PDZ2(160)G–(246)S	+	++++	Histidine

Binding was measured by the yeast mating assay, with the PDZ domain serving as the interactor and the receptor C terminus the bait. Mating was carried out according to the manufacturer's (Clonetech) instructions on plates with various concentrations of aminotriazole (AT). Relative strengths of interaction were determined by the maximum AT concentration that permitted a ß-galactoside–positive signal. 0 mM AT, +; 2.5 mM AT, ++; 10 mM AT, ++++; no signal on 0 mM AT, −.

* Receptor C terminal domain sequences are given in Table 1.

** The PDZ domain αB1 amino acid assignment is given in Figure 1B. See Songyang et al. (1997) for PDZ domain residue nomenclature.

Synaptic Location of ABP

ABP is expressed in diverse brain regions, including pyramidal cells of cortex and hippocampus, and in striatum, brainstem, and spinal cord. Expression in stellate

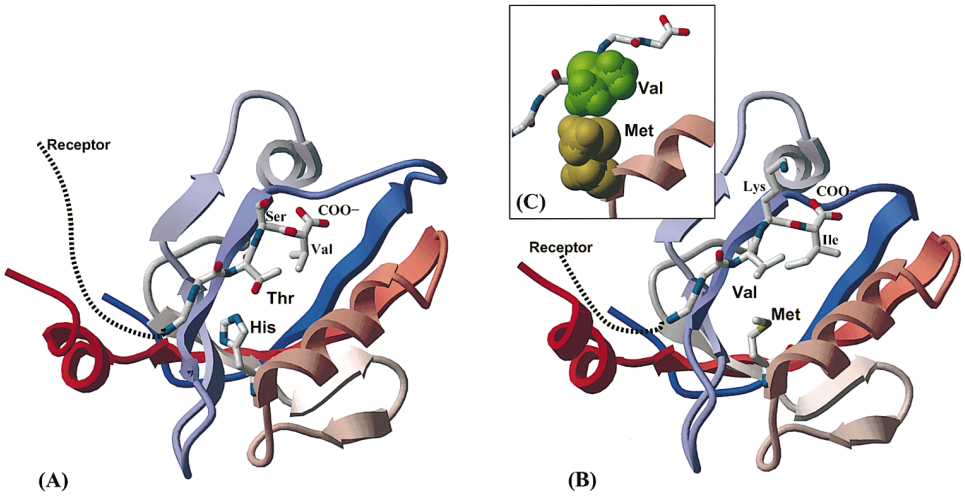

Figure 6. Molecular Model of Interaction between Two Types of PDZ Domains and Receptor C Termini

(A) A crystallographic structure of PDZ3 from PSD-95 (ribbon) complexed with a pentapeptide (balls and sticks).

(B) A model of PDZ5 from ABP with bound GluR2 C terminus. Residues Met 569 of ABP and Val −2 of GluR2 can form a hydrophobic contact in the lowest energy conformation.

(C) A space-filling representation of the contact. Ribbons on (A) and (B) are colored gradually from N termini (blue) to C termini (red). See text for details.

cells of the cerebellum and in nonpyramidal cells in forebrain suggest that ABP is also present in some GABAergic interneurons.

ABP displays a punctate dendritic pattern in cortical pyramidal cells, suggesting a synaptic localization. In neuropil throughout the brain, ABP is also found in punctate structures. Consistent with these observations, ABP is found by electron microscopy to concentrate at the PSD. It copurifies with GluR2 in the subcellular PSD fraction of rat forebrain and binds specifically to GluR2/3 via PDZ domains. All of these observations support a synaptic function for ABP involving interaction with AMPA receptors through GluR2/3 subunits.

Parallel Systems for Receptor Interaction

Like ABP, PSD-95 copurifies with the PSD fraction (Cho et al., 1992) and can be localized at the synaptic membrane (Kim et al., 1995; Topinka and Bredt, 1998). The protein interactions of ABP and the PSD-95 family are also very similar. ABP and GRIP bind to GluR2/3 C termini via PDZ domains (Dong et al., 1997; this report). Similarly, the PDZ domains of PSD-95 bind to NMDA receptor C termini (Kornau et al., 1995; Niethammer et al., 1996). Both families can also multimerize among themselves. S_{II}, which contains PDZ domains 4, 5, and 6 of ABP, can form multimers with itself or with GRIP, as shown by coimmunoprecipitation from 293T cells. Because S_{II} binds to ABP itself and to GRIP in yeast two-hybrid assays, the interaction is most likely direct. Coexpression of ABP and GRIP in COS7 cells causes redistribution of both proteins into large aggregates. PSD-95 also forms homomultimers via its N-terminal domain (Hsueh et al., 1997), and it forms heteromultimers with Chapsyn 110, although the heteromultimers do not form large aggregates on coexpression (Kim et al., 1996). The similarities of the locations and binding properties of these two receptor-interacting families suggest that ABP and GRIP play a role for the AMPA receptor analogous to that provided for the NMDA receptor by the PSD-95 family.

Table 3. Yeast Interaction Assay of Binding of ABP Domains to ABP and GRIP

	ABP or GRIP Interaction Phenotype	
ABP Domain	ABP	GRIP
S_I	−	−
L_1	−	−
L_1S_{II}	+	+
S_{II}	+	+

Binding was measured by the yeast mating assay using the Matchmaker Two kit (Clonetech) according to manufacturer's instructions. Matings were performed on 10 mM aminotriazole (AT) plates. The designated domains of ABP were used as bait, and the original yeast two-hybrid screen isolates of ABP(57)L–(822)F and GRIP(363)A–(1112)L residues were used as interactor. A positive β-galactoside signal is shown by + and a negative by −.

Differential Synaptic Properties of ABP/GRIP and PSD-95

Studies with cultured neurons indicate that NMDA and AMPA receptors are localized at synapses by different mechanisms. In culture, NMDA receptors cluster on dendritic shafts at 2–5 days in vitro, well before AMPA receptors first cluster on spines at 9–10 days (Rao et al., 1998). The more diffuse appearance of AMPA receptors relative to the punctate appearance for the NMDAR, even after clustering, indicates a different distribution of the two receptors at the postsynaptic membrane (Allison et al., 1998). Synaptic differences are also observed by electron microscopy, which shows that AMPA receptors are scattered across the postsynaptic region, while NMDA receptors are collected into a central cluster

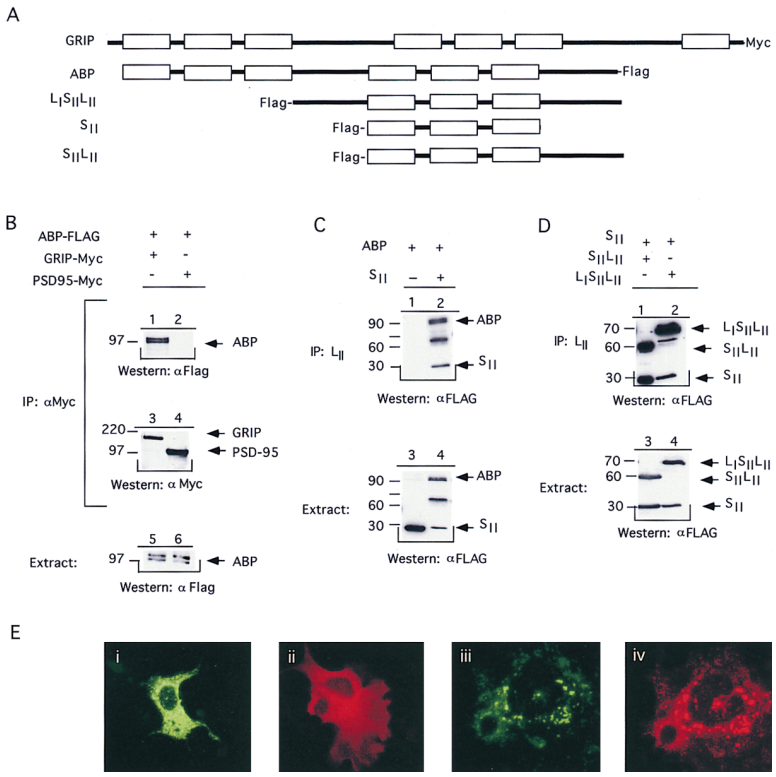

Figure 7. ABP Dimerizes with Itself and GRIP via PDZ Domain S_{II} but Does Not Bind PSD-95

(A) Schematic diagram of ABP and its fragments used for assaying the dimerization activity of ABP.

(B) 293T cells were transfected with full-length ABP and GRIP or PSD-95 as indicated and then immunoprecipitated with myc antibody. The precipitation of ABP was assayed by immunoblotting with FLAG antibody (lanes 1 and 2). The same immunoprecipitated extract was probed for presence of GRIP or PSD-95 by immunoblotting with myc antibody (lanes 3 and 4). Ten percent of input cell extract used for immunoprecipitation was probed with FLAG antibody to confirm the presence of ABP (lanes 5 and 6). ABP selectively dimerizes with GRIP. 293T cells were transfected with full-length ABP and its various deletion constructs (all FLAG-tagged), as indicated, and then immunoprecipitated with ABP L_2 sera. The precipitation of ABP and its deletion constructs was detected by immunoblotting with FLAG antibody.

(C) Specificity of the ABP L_2 sera was assayed by expressing S_{II}, which lacks L_2, and immunoprecipitating with ABP L_2 sera (lanes 1 and 3). S_{II} specifically interacts with full-length ABP, as it is immunoprecipitated by ABP L_2 sera only in the presence of full-length ABP (lanes 2 and 4). This indicates that ABP homodimerizes via S_{II}.

(D) To assay for S_{II} homodimerization, S_{II} was coexpressed with S_{II}–L_2 and L_1–S_{II}–L_2 (lanes 3 and 4). S_{II} was precipitated by both S_{II}–L_2 and L_1–S_{II}–L_2 (lanes 1 and 2), indicating that ABP S_{II} can dimerize with itself.

(E) COS7 cells were transfected with ABP alone (*i*), myc-tagged GRIP alone (*ii*), or with both *ABP* and *GRIP-myc* cDNA (*iii* and *iv*). ABP was detected by rabbit α ABP L_2 antibody (green) and GRIP with mouse anti-myc epitope (red). ABP or GRIP immunoreactivity alone has the appearance of fine aggregates (α myc immunoreactivity was stronger and hence gave the impression of being more uniform). Coexpression of ABP and GRIP resulted in redistribution of ABP and GRIP into large aggregates, which were visualized in nearly 50% of cells coexpressing ABP and GRIP. This suggests that ABP and GRIP can homo- or heteromultimerize to form large scaffold-like complexes.

(Kharazia and Weinberg, 1997; Somogyi et al., 1998). Indeed, it has been suggested (Allison et al., 1998) that AMPA receptors are not directly linked to the cytoskeleton but are "corralled" by neighboring structures into the spine head. In contrast, NMDA receptors appear to be firmly anchored to the macromolecular, cytoskeletal PSD matrix by association with PSD-95 family proteins (Allison et al., 1998). The formation of a tight macromolecular complex between PSD-95 and the NMDA receptor is likely to reflect properties of the PSD-95 and NMDA receptor interaction itself, since the NMDA receptor is readily clustered in heterologous cells by PSD-95 or Chapsyn 110 (Kim et al., 1996). In contrast, under similar conditions, we have not detected clustering of the AMPA receptor by ABP (S. S. and E. Z., unpublished data), although ABP interactions with GluR2 are readily detected in heterologous cells (Figure 5A). It is not yet known whether the heteromultimers of ABP and GRIP can cluster AMPA receptors. ABP does not interact with PSD-95 in heterologous cells (Figure 7B), and thus ABP–AMPA receptor complexes may not link directly to the subsynaptic matrix through an interaction with PSD-95 itself. This may account for the more diffuse synaptic localization of the AMPA receptor, the receptor's relative ease of detergent extraction (Allison et al., 1998), and its greater fluidity at synapses (Rao et al., 1998) in comparison to NMDA receptors.

Distinctive Hydrophobic Bonding of GluR2/3 to ABP

Central to the roles of ABP/GRIP and the PSD-95 family in synaptic interaction with the AMPA and NMDA receptors, respectively, is the ability of anchoring proteins to recognize their target receptors selectively. The current work explains the molecular basis for this recognition specificity. We have shown that PDZ domains 3, 5, and 6 of ABP bind the AMPA receptor via the V-X-I motif at the AMPA receptor C terminus. Both mutagenesis and molecular modeling indicate that the CH_3 moieties of the Val −2 side chain form a critical interaction with αB1 Met and Leu residues of ABP PDZ domains. The binding of GluR2 to ABP is a class II PDZ–protein interaction. In contrast, the PSD-95 family employs a class I interaction that is dependent upon the Ser/Thr residue at −2 of the NMDA receptor C terminus binding to His at the αB1 position of the PDZ domain through a hydrogen bond (Doyle et al., 1996).

Synaptic Targeting of AMPA and NMDA Receptors

The ABP/GRIP and PSD-95 families bind the AMPA and the NMDA receptors, respectively. The parallel but separate molecular interactions of the ABP/GRIP and PSD-95 families provide a basis for the formation of functionally specialized synaptic scaffolds for AMPA and NMDA receptors. Thus far, the mechanism that directs the AMPA

receptor to the synapse is not known. However, ABP and GRIP are candidate agents in this mechanism. Protein localization at synapses involves protein recognition between pre- and postsynaptic membranes. Recently, PSD-95 has been shown to bind neuroligin (Irie et al., 1997), a postsynaptic cell adhesion molecule that binds to presynaptic neurexins across the synaptic cleft. The presence of multiple PDZ domains in ABP may also enable it to bind additional proteins that, like the proposed function of neuroligan for alignment of PSD-95/NMDAR complexes, may contribute to AMPA receptor synaptic localization or otherwise regulate AMPA receptors during synaptogenesis or synaptic modification.

Experimental Procedures

Yeast Two-Hybrid Screen and cDNA Cloning

The last 50 amino acids of GluR2 were cloned in the vector pAS2 by PCR and used as bait in the MATCHMAKERII kit (Clonetech), following the instructions of the manufacturer, to screen an adult rat brain library in pGAD10 (Clonetech). Approximately 1 million clones were screened. Three proteins containing PDZ domains were isolated and studied further. Two overlapping positive clones encoded nucleotides 461–5422 of the *ABP* mRNA. RACE (5′) was performed on the PGAD10 library DNA by an antisense primer (CTG CAG GGT GGC TAT TGC GG) designed to known ABP sequence and both upstream- and downstream-flanking pGAD10 primers. PCR was performed for 35 cycles with hot start on RoboCycler gradient 40 (Stratagene). The PCR products were run on 2% agarose gels and electroblotted to Genescreen Plus Nylon membrane and probed with a ^{32}P-labeled internal ABP-specific probe (GGG CCA CCA GGC CGC ACG TA). Hybridizing PCR reactions were gel purified (Qiaex II, QIAGEN). The purified fragments were TA cloned (Invitrogen), and positive clones were identified by hybridization with the same probe as above. The largest insert (PSD10) that had the initiator methionine and an in-frame termination codon also provided nucleotides 1–460. PSD10 linearized with Pst1 was mixed with yeast two-hybrid–derived ABP vector, and PCR was done for 20 cycles with an upstream primer to PSD10 and a downstream C-terminal FLAG-tagged primer to the terminator of ABP. The PCR product was restricted with EcoRI and electrophoresed on a 0.75% agarose gel. The 2.8 kb band was ligated into the EcoRI site of pCDNA3 (Invitrogen).

The *GRIP* mRNA sequence was deduced from a single yeast screen clone and additional clones identified by colony hybridization.

The specificity of interaction between two potentially interacting proteins was determined by yeast mating/yeast interaction assays according to the instructions of the manufacturer also (Clonetech).

Generation of Antiserum

ABP L_2 antibody was generated by immunization of rabbits with a 16 amino acid peptide (RSVTPQEWRSSRLKSSC) from the L_2 region, with an extra Cys appended at the C terminus that was conjugated to keyhole limpet hemocyanin (KLH) with glutaraldehyde by using Sulfo-SMCC (pH 7.2) (ANASPEC). Conjugated peptides were used to immunize New Zealand white rabbits. Antibodies that recognize ABP were affinity purified on a sepharose peptide column (ANASPEC). Fractions were eluted from the peptide column with 0.1 M glycine (pH 2.5) and immediately neutralized with 1 M Tris (pH 8). Appropriate fractions were pooled and dialyzed overnight in PBS, and protein concentration was estimated by BioRad Protein Assay.

Cell Transfection and Immunoprecipitation

For expression in HEK 293T cells by transfection, *ABP* cDNAs were subcloned in the CMV-FLAG vector (Kodak). The wild-type *GluR2* and *GluR1* cDNAs (gift of J. Boulter and S. Heinemann, Salk Institute) were expressed from pcDNA1 (Invitrogen). The wild-type *PSD-95* cDNA (gift of M. Sheng) was expressed from GW1-CMV mammalian expression vector. The wild-type GRIP was expressed from pcDNA3.1 (Invitrogen). The GluR2 site-directed mutants were constructed in pcDNA3 by PCR. All mutants were confirmed by sequencing. In experiments using the *GluR2* site-directed mutants, the wild-type GluR2 was expressed from pcDNA3. Cells were transfected with 20 μg of DNA per 10 cm dish by the calcium phosphate method. Cells were solubilized in immunoprecipitation buffer (25 mM HEPES [pH 7.5], 2 mM EDTA, 2 mM EGTA, 150 mM NaCl, 1% Triton, 100 μg/ml phenylmethylsulfonyl fluoride [PMSF], 2.5 μg/ml aprotinin, and 0.5 μg/ml leupeptin). Immunoprecipitation was done with 5 μg/sample of anti-FLAG antibody (Kodak) or 1 μg/sample of other antibodies. Immunoprecipitates were collected by protein A/G-sepharose, separated by 8% SDS-PAGE gel, and analyzed by Western blotting.

Protein Preparations

Whole rat brains (adult or developing) were resuspended in five volumes of resuspension buffer (0.1 M NaCl, 10 mM Tris [pH 7.6], 1 mM EDTA [pH 8], 1 μg/ml aprotinin, and 100 μg/ml PMSF). Brain tissue was homogenized, and the lysate was spun at 1,000 × g for 10 min. The protein concentration was assayed by BioRad Protein Assay. To obtain whole-cell protein samples of different brain tissues, the tissues from (8-week-old) rats were homogenized in 25 mM HEPES (pH 7.4), 2 mM EGTA, and 2 mM EDTA buffer containing protease inhibitors (0.2 mM PMSF, 1 μg/ml aprotinin, 1 mM benzamidine, 10 μg/ml leupeptin, and 10 μg/ml pepstatin). The lysate was spun at 1,000 × g for 5 min, and the protein concentration was measured by Bradford assay. Proteins were fractionated by SDS-PAGE.

Subcellular Fractions

Synaptosomal fractions were prepared as described (Carlin et al., 1980). Briefly, six 2-month-old rats were decapitated, and tissue (from cortex) was homogenized in buffer A (0.32 M sucrose, 1 mM $NaHC0_3$, 1 mM $MgCl_2$, and 0.5 mM $CaCl_2$) at 40 ml/10 g. The resulting lysate was diluted to 10% (weight/volume) in buffer A and centrifuged at 1,400 × g for 10 min. The supernatant was collected and recentrifuged at 13,800 × g for 10 min. The pellet was resuspended in buffer B (0.32 M sucrose and 1 mM $NaHCO_3$) at 24 ml/10 g of starting protein. The lysate was loaded at top of sucrose gradients (6 ml of protein and 8 ml each of 0.85, 1.0, and 1.2 M sucrose) and centrifuged at 82,500 × g for 120 min. The synaptosomes were collected from 1.0 and 1.2 M sucrose interface, diluted four times in buffer B, and spun at 13,800 × g for 15 min. The synaptosomal pellet was lysed with hypotonic buffer C (10 mM HEPES [pH 7.4], 2 mM EDTA, 2 mM EGTA, 0.2 mM PMSF, 1 μg/ml aprotinin, 1 mM benzamidine, 1 mM leupeptin, and 10 μg/ml pepstatin), and the full synaptosomal fraction was collected. The rest of the lysate was centrifuged at 30,000 × g for 30 min, and the supernatant was saved as a synaptosomal-cytosolic fraction. The pelleted membranes were resuspended at 2 ml/10 g of starting tissue in buffer D (same as buffer C plus 150 mM NaCl), and the synaptosomal membrane fraction was collected. The rest of the protein was diluted 1:1 in buffer E (same as buffer D plus 2% Triton X-100) and spun 100,000 × g for 30 min. The resulting pellet was collected as the PSD fraction.

Western Blot Analysis

Western blots were probed with C terminus antibody for GluR2/3 (Chemicon), N terminus GluR2 monoclonal antibody (Chemicon) for site-directed mutants of GluR2, rabbit polyclonal antibody (Chemicon) for GluR1 and c-myc 9E10 (Santa Cruz Biotechnology) for myc-tagged proteins, and M2 anti-FLAG antibody (Kodak) for FLAG-tagged proteins. Affinity-purified ABP L_2 antibody was used to detect wild-type ABP and ABP in the brain. All antibodies were used at the concentration of 1 μg/ml, except for anti-FLAG antibody, which was used at 3.2 μg/ml. Blots were visualized by enhanced chemiluminescence with the ECL Kit (Amersham).

Immunofluorescence on COS7 Cells

COS7 cells were transfected with the designated plasmids by the Lipofectamine method (GIBCO-BRL) at 60%–70% confluency on poly-lysine–coated coverslips. Transfected cells were incubated with neuron-conditioned medium for 48 hr. Transfected COS7 cells were fixed in 70% acetone and 30% methanol. Cells were stained

by using the designated primary antibody at 1 μg/ml and secondary antibody (Calbiochem) at a 1:200 dilution. Immunofluorescence was visualized with a Zeiss Axiophot microscope. Imaging was done by Adobe Photoshop.

Immunocytochemistry on Brain Sections

Male Sprague-Dawley rats (300–350 g) were anesthetized with pentobarbital (60 mg/kg) and perfused intraaortically with fixative containing 4% freshly depolymerized paraformaldehyde (for immunoperoxidase) or 2% paraformaldehyde, 2% glutaraldehyde, and 0.1% picric acid (for immunogold) in 0.1 M phosphate buffer (PB) (pH 7.4) after a brief flush with heparinized saline. Parasagittal and coronal sections (40 μm thick) from brain and transverse sections from spinal cord at lumbar level were cut on a Vibratome and collected in PB.

Preembedding immunoperoxidase for laminin (LM) was performed by using affinity-purified ABP L_2 sera. Sections were pretreated sequentially in 50% ethanol (to permeabilize the tissue) and 3% hydrogen peroxide in PBS (to inactivate endogenous peroxidases) and then blocked in 10% normal donkey serum. Sections were incubated overnight in primary antibody (diluted 1:300–1:600 in PBS), 2 hr in biotinylated donkey anti-rabbit serum (Jackson; 1:200), and then in ExtrAvidin peroxidase complex for 1 hr (Sigma; 1:5,000). After revealing peroxidase activity with diaminobenzidine (DAB) or nickel-enhanced diaminobenzidine, sections were mounted on gelatin-coated slides and examined with bright field. No staining was seen in the absence of primary antibody.

For electron microscopy (EM), sections were first embedded as described (Phend et al., 1995). Briefly, sections on ice were treated sequentially in 1% tannic acid in 0.1 M maleate buffer (MB) (pH 6.0), 1% uranyl acetate, 0.5% iridium tetrabromide (Pfaltz and Bauer, Waterbury, CT), 50% and 70% ethanol, 1% phenylenediamine hydrochloride in 70% ethanol, and 1% uranyl acetate in 70% ethanol and then dehydrated in 80%, 95%, and 100% ethanol. Sections were then immersed in propylene oxide and infiltrated with Epon-Spurr resin. Following overnight infiltration in resin, sections were sandwiched between strips of Aclar plastic film, flattened between microscopic slides, and polymerized at 60°C for 36 hr. Chips from layers II–III of S-1 cortex, the CA2 region of hippocampus, or the molecular layer of cerebellar cortex were glued onto plastic blocks. Thin sections (~90 nm) were cut and collected on 300-mesh uncoated nickel grids and treated with Quick-Coat (Kiyota Express, Elk Grove, IL) for improved section adhesion.

For postembedding immunogold, we used affinity-purified ABP L_2 sera following steps as previously described (Phend et al., 1995). Briefly, grids were washed with Tris-buffered saline containing 0.005% Tergitol NP-10 (pH 7.6) (TBS/T), incubated overnight at 37°C in primary antibody (1:100), rinsed in TBS/T (pH 7.6), transferred to TBS/T (pH 8.2), and incubated in secondary gold-conjugated antibody (IgG conjugated to 18 nm gold particles (Jackson ImmunoResearch) diluted 1:20 in TBS/T. Following immunocytochemical processing, grids were air dried and poststained with uranyl acetate and Sato's lead and examined with a JEOL CX200 at 80 kV. For quantitative analysis of gold particles, photographs of 20 random fields from layers II–III of cerebral cortex containing at least one clearly defined synapse with at least one gold particle within 100 nm of the active zone (AZ) were taken for each of three animals. Negatives (at 40,000× original magnification) were digitized at 400 dpi on a flatbed scanner, and all particles within 200 nm of the synapse were measured by using NIH Image software. "Axodendritic" distances were defined as the distance from the center of each particle to the outer leaflet of the postsynaptic membrane. "Lateral" distances were measured from the center of each particle to a line drawn perpendicular to the edge of each side of the AZ. Lateral edges of the AZ were defined by the points of disappearance of the PSD. In perforated synapses, the entire length of the synapse, including all fragments with PSD and all perforations, was measured as a single AZ. Lateral positions of gold particles were normalized by computing the absolute value of the ratio of the difference of distances to the two sides of the AZ, divided by the total length of the AZ.

Acknowledgments

We thank S. Heineman and J. Boulter for AMPA receptor cDNA plasmids, M. Sheng for the *PSD-95* cDNA clone, R. MacKinnon for the PSD-95 PDZ3 crystal structure file, and T. Serra for preparation of the manuscript. Computing was supported by the New York University Research Computing Resource. This work was supported by Department of Energy grants DE-GF02–96ER6226 (to R. A.) and NS29879 (to R. J. W.) and by the Howard Hughes Medical Institute. S. S. and B. S. were supported by National Institutes of Health grant AG13620 (to E. B. Z). R. A. is a member of the Skirball Institute of New York University Medical Center. P. O., F. S. V., G. I., C. D., and S. DeS. are Associates and E. B. Z. is an Investigator of the Howard Hughes Medical Institute.

Received April 22, 1998; revised July 8, 1998.

References

Allison, D.W., Gelfand, V.I., Spector, I., and Craig, A.M. (1998). Role of actin in anchoring postsynaptic receptors in cultured hippocampal neurons: differential attachment of NMDA versus AMPA receptors. J. Neurosci. *18*, 2423–2436

Anderson, J.M. (1996). Cell signaling: MAGUK magic. Curr. Biol. *6*, 382–384.

Cabral, J.H., Petosa, C., Sutcliffe, M.J., Raza, S., Byron, O., Poy, F., Marfatia, S.M., Chishti, A.H., and Liddington, R.C. (1996). Crystal structure of a PDZ domain. Nature *382*, 649–652.

Cardozo, T., Totrov, M., and Abagyan, R. (1995). Homology modeling by the ICM method. Proteins *23*, 403–414.

Carlin, R.K., Grab, D.J., Cohen, R.S., and Siekevitz, P. (1980). Isolation and characterization of postsynaptic densities from various brain regions: enrichment of different types of postsynaptic densities. J. of Cell Biol. *86*, 831–845.

Cho, K.O., Hunt, C.A., and Kennedy, M.B. (1992). The rat brain postsynaptic density fraction contains a homolog of the Drosophila discs–large tumor suppressor protein. Neuron *9*, 929–942.

Dong, H., O'Brien, R.J., Fung, E.T., Lanahan, A.A., Worley, P.F., and Huganir, R.L. (1997). GRIP: a synaptic PDZ domain–containing protein that interacts with AMPA receptors [see comments]. Nature *386*, 279–284.

Doyle, D.A., Lee, A., Lewis, J., Kim, E., Sheng, M., and MacKinnon, R. (1996). Crystal structures of a complexed and peptide-free membrane protein–binding domain: molecular basis of peptide recognition by PDZ. Cell *85*, 1067–1076.

Ehlers, M.D., Mammen, A.L., Lau, L.F., and Huganir, R.L. (1996). Synaptic targeting of glutamate receptors. Curr. Opin. Cell Biol. *8*, 484–489.

Fields, S., and Song, O. (1989). A novel genetic system to detect protein–protein interactions. Nature *340*, 245–246.

Gomperts, S.N. (1996). Clustering membrane proteins: it's all coming together with the PSD-95/SAP90 protein family. [Review]. Cell *84*, 659–662.

Hampson, D.R., Huang, X.P., Oberdorfer, M.D., Goh, J.W., Auyeung, A., and Wenthold, R.J. (1992). Localization of AMPA receptors in the hippocampus and cerebellum of the rat using an anti-receptor monoclonal antibody. Neuroscience *50*, 11–22.

Hayashi, Y., Ishida, A., Katagiri, H., Mishina, M., Fujisawa, H., Manabe, T., and Takahashi, T. (1997). Calcium- and calmodulin-dependent phosphorylation of AMPA type glutamate receptor subunits by endogenous protein kinases in the post-synaptic density. Brain Res. Mol. Brain Res. *46*, 338–342.

Hollmann, M., and Heinemann, S. (1994). Cloned glutamate receptors. Annu. Rev. Neurosci. *17*, 31–108.

Hsueh, Y.P., Kim, E., and Sheng, M. (1997). Disulfide-linked head-to-head multimerization in the mechanism of ion channel clustering by PSD-95. Neuron *18*, 803–814.

Irie, M., Hata, Y., Takeuchi, M., Ichtchenko, K., Toyoda, A., Hirao, K., Takai, Y., Rosahl, T.W., and Sudhof, T.C. (1997). Binding of neuroligins to PSD-95. Science *277*, 1511–1515.

Isaac, J.T., Nicoll, R.A., and Malenka, R.C. (1995). Evidence for silent synapses: implications for the expression of LTP. Neuron *15*, 427–434.

Jonas, P., Racca, C., Sakmann, B., Seeburg, P.H., and Monyer, H. (1994). Differences in Ca^{2+} permeability of AMPA-type glutamate receptor channels in neocortical neurons caused by differential GluR-B subunit expression. Neuron *12*, 1281–1289.

Kennedy, M.B. (1997). The postsynaptic density at glutamatergic synapses. Trends Neurosci. *20*, 264–268.

Kharazia, V.N., and Weinberg, R.J. (1997). Tangential synaptic distribution of NMDA and AMPA receptors in rat neocortex. Neurosci. Lett. *238*, 41–44.

Kim, E., Niethammer, M., Rothschild, A., Jan, Y.N., and Sheng, M. (1995). Clustering of Shaker-type K^+ channels by interaction with a family of membrane-associated guanylate kinases. Nature *378*, 85–88.

Kim, E., Cho, K.O., Rothschild, A., and Sheng, M. (1996). Heteromultimerization and NMDA receptor–clustering activity of Chapsyn-110, a member of the PSD-95 family of proteins. Neuron *17*, 103–113.

Kim, E., Naisbitt, S., Hsueh, Y.P., Rao, A., Rothschild, A., Craig, A.M., and Sheng, M. (1997). GKAP, a novel synaptic protein that interacts with the guanylate kinase–like domain of the PSD-95/SAP90 family of channel clustering molecules. J. Cell Biol. *136*, 669–678.

Kistner, U., Wenzel, B.M., Veh, R.W., Cases, L.C., Garner, A.M., Appeltauer, U., Voss, B., Gundelfinger, E.D., and Garner, C.C. (1993). SAP90, a rat presynaptic protein related to the product of the *Drosophila* tumor suppressor gene dlg-A. J. Biol. Chem. *268*, 4580–4583.

Kornau, H.C., Schenker, L.T., Kennedy, M.B., and Seeburg, P.H. (1995). Domain interaction between NMDA receptor subunits and the postsynaptic density protein PSD-95. Science *269*, 1737–1740.

Lau, L.F., Mammen, A., Ehlers, M.D., Kindler, S., Chung, W.J., Garner, C.C., and Huganir, R.L. (1996). Interaction of the N-methyl-D-aspartate receptor complex with a novel synapse-associated protein, SAP102. J. Biol. Chem. *271*, 21622–21628.

Liao, D., Hessler, N.A., and Malinow, R. (1995). Activation of postsynaptically silent synapses during pairing-induced LTP in CA1 region of hippocampal slice. Nature *375*, 400–404.

Malenka, R.C., and Nicoll, R.A. (1997). Silent synapses speak up. Neuron *19*, 473–476.

Maren, S., Tocco, G., Standley, S., Baudry, M., and Thompson, R.F. (1993). Postsynaptic factors in the expression of long-term potentiation (LTP): increased glutamate receptor binding following LTP induction *in vivo*. Proc. Natl. Acad. Sci. USA *90*, 9654–9658.

McBain, C.J., and Mayer, M.L. (1994). N-methyl-D-aspartic acid receptor structure and function. Physiol. Rev. *74*, 723–760.

Naisbitt, S., Kim, E., Weinberg, R.J., Rao, A., Yang, F.C., Craig, A.M., and Sheng, M. (1997). Characterization of guanylate kinase–associated protein, a postsynaptic density protein at excitatory synapses that interacts directly with postsynaptic density-95/synapse-associated protein 90. J. Neurosci. *17*, 5687–5696.

Niethammer, M., Kim, E., and Sheng, M. (1996). Interaction between the C terminus of NMDA receptor subunits and multiple members of the PSD-95 family of membrane-associated guanylate kinases. J. Neurosci. *16*, 2157–2163.

Phend, K.D., Rustioni, A., and Weinberg, R.J. (1995). An osmium-free method of epon embedment that preserves both ultrastructure and antigenicity for post-embedding immunocytochemistry. J. Histochem. Cytochem. *43*, 283–292.

Rao, A., Kim, E., Sheng, M., and Craig, A.M. (1998). Heterogeneity in the molecular composition of excitatory postsynaptic sites during development of hippocampal neurons in culture. J. Neurosci. *18*, 1217–1229.

Seeburg, P.H. (1996). The role of RNA editing in controlling glutamate receptor channel properties. J. Neurochem. *66*, 1–5.

Sheng, M., and Wyszynski, M. (1997). Ion channel targeting in neurons. Bioessays *19*, 847–853.

Somogyi, P., Tamás, G., Lujan, R., and Buhl, E.H. (1998). Salient features of synaptic organisation in the cerebral cortex. Brain Res. Rev. *26* (http://www1.elsevier.com/journals/bres/menu.htm).

Songyang, Z., Fanning, A.S., Fu, C., Xu, J., Marfatia, S.M., Chishti, A.H., Crompton, A., Chan, A.C., Anderson, J.M., and Cantley, L.C. (1997). Recognition of unique carboxyl-terminal motifs by distinct PDZ domains. Science *275*, 73–77.

Topinka, J.R., and Bredt, D.S. (1998). N-terminal palmitoylation of PSD-95 regulates association with cell membranes and interaction with K^+ channel $K_{v1}.4$. Neuron *20*, 125–134.

Ziff, E.B. (1997). Enlightening the postsynaptic density. Neuron *19*, 1163–1174.

GenBank Accession Number

The sequence of ABP has been submitted to GenBank under accession number AF090113.